Bioactive Materials 6 (2021) 3300–3313

Contents lists available at ScienceDirect

Bioactive Materials

journal homepage: www.sciencedirect.com/journal/bioactive-materials

Cascaded amplification of intracellular oxidative stress and reversion of multidrug resistance by nitric oxide prodrug based-supramolecular hydrogel for synergistic cancer chemotherapy

Jimin Zhang [a,1], Meigui Deng [a,1], Xiaoguang Shi [b], Chuangnian Zhang [b], Xiongwei Qu [a], Xiuli Hu [a,*], Weiwei Wang [b,**], Deling Kong [c], Pingsheng Huang [b,***]

[a] Hebei Key Laboratory of Functional Polymers, National-Local Joint Engineering Laboratory for Energy Conservation of Chemical Process Integration and Resources Utilization, School of Chemical Engineering and Technology, Hebei University of Technology, Tianjin, 300130, China
[b] Tianjin Key Laboratory of Biomaterial Research, Institute of Biomedical Engineering, Chinese Academy of Medical Sciences and Peking Union Medical College, Tianjin, 300192, China
[c] State Key Laboratory of Medicinal Chemical Biology, College of Life Sciences, Nankai University, Tianjin, 300071, China

ARTICLE INFO

Keywords:
NO prodrug
Supramolecular hydrogel
Oxidative stress
Multidrug resistance
Synergistic therapy

1. Introduction

Chemotherapy is the traditional treatment for clinical cancer patient [1,2]. However, the therapeutic effect is often severely limited by the multidrug resistance (MDR) [3,4], which was commonly mediated by inactivating drugs, increasing efflux, stimulating DNA repair mechanisms, and/or activating detoxification pathways [5–7]. Recent studies are committing to develop reasonable strategies for intervention of the molecular pathways mediating MDR, of which P-glycoprotein (P-gp) has been widely investigated [8]. So far, several kinds of P-gp inhibitors, including verapamil [9],vitamin E [10], cyclosporin A [11], and small interfering RNA (siRNA) [12], have been used to increase the intracellular accumulation of chemotherapeutic drugs. However, there is still a vigorous requirement to develop novel bioactive inhibitors, which could not only decrease the expression of P-gp thus increasing the intracellular accumulation of antitumor drugs, but also have effective tumor inhibition effect by its-self.

Nitric oxide (NO), an endogenous gaseous molecular messenger, demonstrated great potential in inhibiting carcinogenesis and tumor growth [13,14]. Increasing evidences showed that NO could directly kill cancer cells through multiple pathways [15], including producing of oxidative and nitrosative stress [16], damage mitochondria and DNA [17], enhance lipid peroxidation and impaired cellular function [18]. In particular, oxidative stress induced antitumor mechanism was mainly attributed to mitochondrion-mediated apoptotic pathways [19]. Firstly, NO induced ROS elevation by down-regulate the core proteins of mitochondria respiratory chain (MRC) complex I and IV, resulting in the suppression of MRC complex I and IV activity and further ROS production [20]. Then, the upregulated ROS could induce oxidative stress-mediated mitochondrial dysfunction, such as the loss of mitochondrial membrane potential, and eventually mitochondrion-mediated apoptotic pathway was turn on [21]. Importantly, recent studies demonstrated that NO has chemosensitization effect by decreasing the P-gp expression levels [22,23]. Hence, when combined with antitumor

Peer review under responsibility of KeAi Communications Co., Ltd.
* Corresponding author.
** Corresponding author.
*** Corresponding author.
E-mail addresses: huxiuli@hebut.edu.cn (X. Hu), wwwangtj@163.com (W. Wang), sheng1989.2008@163.com (P. Huang).
[1] These authors contributed equally to this work.

https://doi.org/10.1016/j.bioactmat.2021.03.005
Received 8 January 2021; Received in revised form 24 February 2021; Accepted 3 March 2021

drugs, NO should have great potential for combating multidrug resistance cancer by direct antitumor effect and indirect chemosensitization effect, achieving synergistic cancer chemotherapy.

So far, several intravenously administrated nano NO delivery systems have been developed [24,25], aiming at realizing tumor target delivery and tumor microenvironment stimuli-triggered NO release, however, the therapeutic effect was often limited by the low tumor accumulation and bioavailability [26,27]. Alternatively, supramolecular hydrogel based on self-assembling peptides has been attracted a great interest in drug delivery systems [28], due to their synthetic accessibility, high bioavailability and smart responsiveness to pathological signals [29,30]. Among them, the integration of peptide gelator with certain bioactive molecules could feasibly modulate the self-assembling behaviors and biological effects, such as induction of cancer cell apoptosis [31,32], immunoregulation [33,34], tissue regeneration [35,36], etc.

Inspired by the virtue of supramolecular hydrogels, herein, a kind of NO prodrug-based oligo-peptide-based hydrogels was developed, which could not only serve as direct therapeutic agent but also provide a facile and effective platform for the codelivery of chemotherapeutic drugs with the capacity of overcoming MDR. As depicted in Scheme 1, the GSH/GST-responsive NO prodrug alkynyl-JSK was conjugated onto the tactical NapFFGEE-N_3 hydrogelator sequence by facile click reaction, obtaining the NO functional peptide (NapFFGEE-JSK), which could self-assemble into nanofiber supramolecular hydrogel due to the non-covalent hydrophobic and hydrogen-bonding interactions. To our consideration, both the NO prodrug JSK and NapFF peptide gelator were hydrophobic, where EE amino acids with two carboxylic acid (COOH) residues were introduced to not only tune the hydrophile-lipophile balance for driving gelation assembly but also provide electrostatic binding point for doxorubicin (DOX). Upon uptake by the MCF-7 ADR cells, the nanofibers were expected to response to the overexpressed GSH/GST and trigger NO release locoregionally and sustainedly, resulting in intracellular amplification of oxidative stress due to the superior GSH consumption and the excellent ROS production synchronously. Subsequently, oxidative stress involved mitochondrion mediated cell apoptotic was expected to achieve excellent antitumor effect. Except from the direct antitumor effect of NO, this supramolecular hydrogel could serve as a facile and effective platform for the codelivery of DOX, which could self-assemble with the polypeptide nanofiber though electrostatic and hydrophobic interactions. This system is expected to achieve GSH/GST triggered NO release and pH-sensitive DOX release in a locoregional and synergetic manner. Based on such design, NO not only killed tumor cells through mitochondrion mediated cell apoptotic pathway, but also sensitized MDR breast cancer cells for DOX by reversing the P-gp mediated efflux pathway, which were expected to obtain synergistic antitumor effect on drug-resistant breast cancer.

2. Experimental methods

2.1. Synthesis of NO prodrug functional peptide NapFFGEE-JSK

First, the peptide NapFFGEE was prepared by typical solid-phase synthesis (SPPS) [32]. Afterwards, the peptide hydrogelator NapFFGEE-N_3 was synthesized by condensation reaction. 1.0 mmol (795.3 mg) of peptide NapFFGEE, 1.1 mmol (416.9 mg) of HBTU and 2.2 mmol of DIPEA (284.4 mg) were dissolved in 2 mL of DMF, then 1.1 mmol of 3-azidopropylamine (100 mg) were added to the above solution. After stirring at room temperature (25 °C) over night, the reaction liquid was directly sent to HPLC purification, finally got about 75% yield. The chemical structure of NapFFGEE-N_3 was determined by ^{1}H NMR.

The NO prodrug alkynyl-JSK was synthesized according to previously reported method [14]. The chemical structures of alkynyl-JSK were verified by ^{1}HNMR. Then, the NO prodrug functional peptide NapFFGEE-JSK was synthesized by click chemistry. Briefly, NapFFGEE-N_3 (1×10^{-3} mol, 1.3 g) was dissolved in H_2O (15 mL) in the presence of $CuSO_4$ (5×10^{-4} mol, 0.125 g) and sodium ascorbate (1×10^{-3} mol, 0.196 g) under the protection of nitrogen atmosphere. Alkynyl-JSK (1.5×10^{-3} mol, 1.58 g) dissolved in THF (5 mL) was added to the peptide solution, which was conducted at 37 °C for 24 h. After the reaction was finished, the products were dialyzed against deionized water. The chemical structure of NapFFGEE-JSK was analyzed by ^{1}H NMR, ATR-FTIR spectroscopy, UV spectrum and Circular dichroism.

2.2. Preparation and characterization of NapFFGEE-JSK hydrogel and NapFFGEE-JSK/DOX hydrogel

NapFFGEE-JSK hydrogel was prepared according to the following process. 2.0 mg of NapFFGEE-JSK and 1.5 equiv. of Na_2CO_3 were firstly suspended in 200 μL phosphate buffer saline (PBS, pH = 7.4), and the

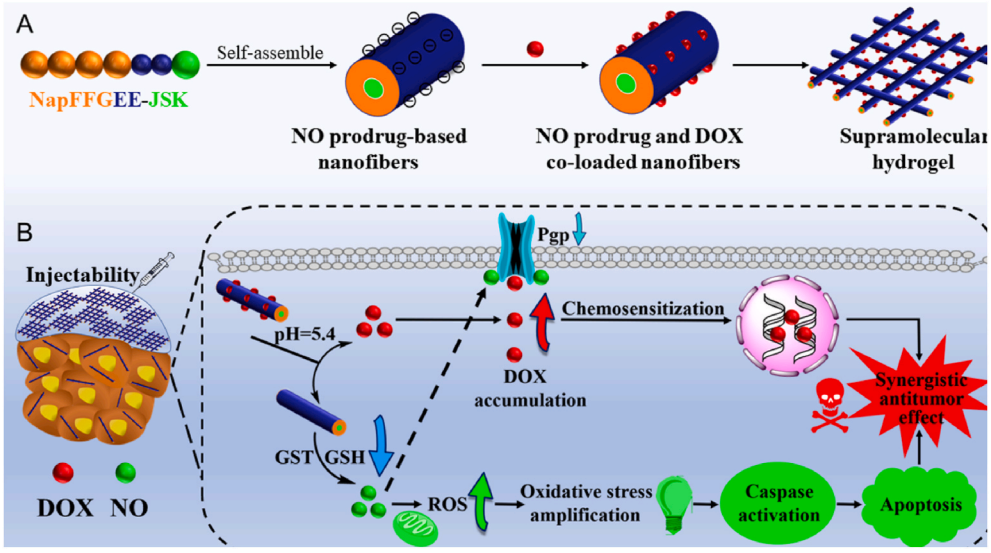

Scheme 1. The design of glutathione/glutathione S-transferase responsive NO prodrug based-supramolecular hydrogel for combating multidrug resistance in synergistic cancer chemotherapy. (A) the formation of NapFFGEE-JSK/DOX supramolecular hydrogel by self-assembly, and further loading with DOX by electrostatic and hydrophobic interactions. (B) The synergistic antitumor mechanism of NapFFGEE-JSK/DOX supramolecular hydrogel for combating multidrug resistance. Firstly, GSH/GST-triggered NO release locoregionally from NapFFGEE-JSK result in intracellular superior GSH depletion and the excellent ROS production, the cascade amplification of oxidative induced mitochondrion mediated cell apoptosis, thereby demonstrating direct antitumor effect. Moreover, in this codelivery system, NO sensitize drug-resistant cancer cells by reversing the P-gp mediated MDR effect, facilitating the intracellular DOX accumulation, which finally resulting in significant synergistic antitumor effect.

suspensions were heated to form clear solutions. Then, the sample was transferred to a 2 mL flat-bottomed vial and cooled to room temperature for gelation.

The DOX loaded NapFFGEE-JSK/DOX hybrid hydrogel was prepared using the same method as NapFFGEE-JSK hydrogel. 0.1 equiv. of DOX was mixed well with NapFFGEE-JSK solution, after gelling process, the hybrid hydrogel was soaked in PBS solution to remove the unbounded DOX. Then, the encapsulation efficiency of DOX in NapFFGEE-JSK/DOX hybrid hydrogel was monitored and calculated with UV spectrum.

The critical micelle concentration (CMC) of NapFFCEE-JSK was studied by dynamic light scattering (DLS). Different concentrations of the NapFFCEE-JSK solution were tested, of which the light scattering intensity was measured. The rheological properties of the hydrogel were investigated on a rheometer (Thermo Scientific HAAKE RheoStress 6000) at 25 °C, at an angular frequency of 6.282 rad/s and strain of 1.0%.

The nanostructure of NapFFGEE-JSK hydrogel was evaluated by Transmission Electron Microscopy (TEM). To study the involvement of electrostatic interactions in the co-assembled hydrogel of DOX and NapFFGEE-JSK, NapFFGEE-JSK/DOX supramolecular hydrogel (1 wt%) was diluted to NapFFGEE-JSK/DOX solution (0.1 wt%) by PBS. Absolute values of zeta potential of the NapFFGEE-JSK/DOX solution was measured on Zetasizer Malvern 3000HS (UK).

2.3. NO release in vitro

Qualitative JSK-decomposition triggered by GSH/GST was monitored by UV spectrum. NapFFGEE-JSK hydrogel or alkynyl-JSK (25 μM) in 3 mL PBS was added appropriate amount of GSH/GST (10 mM GSH and 5 μg/mL GST), and the absorb peak attributed to NO prodrug at 325 nm was monitored.

Quantity of NO release was determined by standard Griess assay. NO release of NapFFGEE-JSK in comparison to alkynyl-JSK (20 μM) was monitored at 37 °C in PBS buffer with different pH in the presence or absence of 10 mM GSH and 5 μg/mL GST. Griess reagent (50 μL) mixed with the 50 μL sample was incubated for 10 min at room temperature. The full wavelength scans were examined by UV spectrum.

Cellular uptake of peptide was evaluated by monitoring FITC-labeled NapFFGEE-FITC peptide. MCF-7 ADR cells (10^5 cells/well) were seeded in 35 mm^2 confocal dishes and incubated for 24 h. Then, the cells were subsequently incubated with NapFFGEE-FITC peptide (60 μM) for 4 h, which were washed with cold PBS, fixed in 4% paraformaldehyde and stained with DAPI. The fluorescence signal of NapFFGEE-FITC peptide was evaluated by confocal laser scanning microscopy.

Intracellular release and distribution of NO in MCF-7 ADR cells was qualitatively monitored with DAF-FM DA probe. The intracellular NO release and distribution were analyzed using confocal laser scanning microscopy. In addition, the sustained NO release of NapFFGEE-JSK hydrogel in MCF-7 ADR cells was tested using the same method with prolonged time point at 2 h, 6 h and 12 h. Furthermore, the quantitative of NO fluorescence intensity was further determined by flow cytometry assay.

2.4. The cytotoxicity and apoptosis assays of NapFFGEE-JSK hydrogel in vitro

The cytotoxicity of NapFFGEE-JSK hydrogel was conducted against MCF-7 ADR cells using CCK-8 assay. MCF-7 ADR cells were cultured and incubated with medium containing NapFFGEE-JSK hydrogel or alkynyl-JSK at serial concentrations of 8, 16, 32, 64, 128, 256 μM for 24, 48, 72 h, respectively. Then cells were collected and the cytotoxicity of MCF-7 ADR cells was determined using CCK-8 assay.

MCF-7 ADR cells (10^4 cells/well) were cultured and incubated with PBS, alkynyl-JSK and NapFFGEE-JSK (62 μM) for 24 h, cells were collected and washed with PBS, and stained with annexin V-fluorescein isothiocyanate (FITC) and propidium iodide for 15 min. The percentage of apoptosis cells was quantified by flow cytometry.

2.5. Intracellular ROS and GSH/GSSG level

MCF-7 ADR cells (10^4 cells/well) were seeded in a 6-well plate for 24 h. After treatment with PBS, alkynyl-JSK, NapFFGEE-JSK hydrogel for 48 h, cells were collected and incubated with serum-free medium containing DCFH-DA for 20 min. DCF fluorescence intensity was determined by flow cytometry. In addition, cells were harvested and lysed by two successive rounds of freezing and thawing. After centrifuging, the supernatant was obtained and analyzed for GSH and glutathione disulfide (GSSG) levels using the GSH and GSSG Assay Kit.

2.6. Measurement of mitochondrial membrane potential and ATP production

Mitochondrial membrane potential was detected by the JC-1Mitochondrial Membrane Potential Assay Kit and analyzed by flow cytometry. MCF-7 ADR cells (10^4 cells/well) were treated with PBS, alkynyl-JSK, NapFFGEE-JSK hydrogel for 48 h. Then, cells were lysed at 4 °C. After centrifuging, the supernatant was obtained and analyzed for ATP levels using an ATP Assay Kit.

2.7. pH-sensitive DOX release in vitro

The pH triggered DOX release from NapFFGEE-JSK/DOX was investigated *in vitro*. DOX release study was carried out by soaking NapFFGEE-JSK/DOX hydrogel in PBS in different pH values of 7.4, 6.4 and 5.0 with or without 10 mM GSH and 5 μg/mL, respectively. To obtain the DOX release profile, 1 mL of NapFFGEE-JSK/DOX hydrogel were incubated in 5 mL of PBS at 37 °C. At scheduled time point. 5 mL of PBS was taken out for testing DOX release by UV spectrum, and another 5 mL fresh PBS was added to proceed experiment.

2.8. Synergistic anticancer effect and mechanism of NapFFGEE-JSK/DOX

The cell cytotoxicity of NapFFGEE-JSK/DOX hybrid hydrogel against MCF-7 ADR cells for 24, 48, 72 h was determined using CCK8 assay. The combination index (CI) values were calculated by Chou-Talalay analysis of the fraction affected (Fa). The apoptosis assays of NapFFGEE-JSK/DOX hybrid hydrogel was conducted using Annexin V-FITC Apoptosis Detection Kit.

To explore the synergistic mechanism of NapFFGEE-JSK/DOX against drug resistant cell, the reverse effect of NO on P-gp expression was studied using western blot analysis. MCF-7 ADR cells were cultured and treatment with PBS, free DOX or NapFFGEE-JSK/DOX (DOX, 5 μg/mL, JSK, 5 μg/mL) for 24 h, respectively. Then the inhibition of P-gp induced enhancing DOX accumulation in MCF-7 ADR cells was further investigated by monitoring DOX fluorescence intensity and distribution by confocal laser scanning microscopy. The quantitative fluorescence intensity of intracellular DOX was further determined by flow cytometry assay. The experiment group was DOX, NapFFGEE-JSK/DOX hydrogel, respectively.

2.9. Antitumor activity in vivo

The *in vivo* antitumor efficiency of NapFFGEE-JSK/DOX hydrogel was assessed in NOD-SCID immune-deficient mice bearing MCF-7/ADR orthotopic xenografts. The injectable hydrogel NapFFGEE-JSK/DOX was prepared firstly according to the following process: 20 mg NapFFGEE-JSK (JSK-based) and 20 mg DOX were firstly suspended in 20 ml phosphate buffer saline (PBS with 1.5 equiv. of Na_2CO_3), the suspensions were heated to form clear solutions and then cooled to room temperature for gelation. Then the tumor with a size of ~50 mm^3 were used for peritumoral injection with division into four groups (n = 5): (1)

control injected with saline, (2) free DOX, (3) NapFFGEE-JSK, (4) NapFFGEE-JSK/DOX. The dose for alkynyl-JSK and DOX for all formulations was 5 mg kg^{-1} and 5 mg kg^{-1} for each injection in the same volume (100 μL), respectively. The mice received two injections at 1 and 7 days respectively over the therapeutic period of two weeks. On the 15th day post treatment, all groups were sacrificed and the tumor tissues were harvested for antitumor efficiency evaluation, including tumor volume, weight. Tissue sections (5 μm in thickness) were harvested and then stained with H&E after deparaffinization. In addition, major organs (including heart, liver, spleen, lung and kidney) were also harvested for the biosafety evaluation of the NapFFGEE-JSK/DOX hydrogel formulation.

3. Results and discussion

3.1. Synthesis and characterization of NapFFGEE-JSK peptide

Supramolecular hydrogels often served as an excellent nanoplatform for drug delivery [37–39]. Nap-FFG has been demonstrated to be a good hydrogelator due to its self-assembling ability from diphenylalanine (FF) with aromatic capping groups [40–42]. To realize the delivery of the hydrophobic NO prodrug (alkynyl-JSK), the Nap-FFG was further

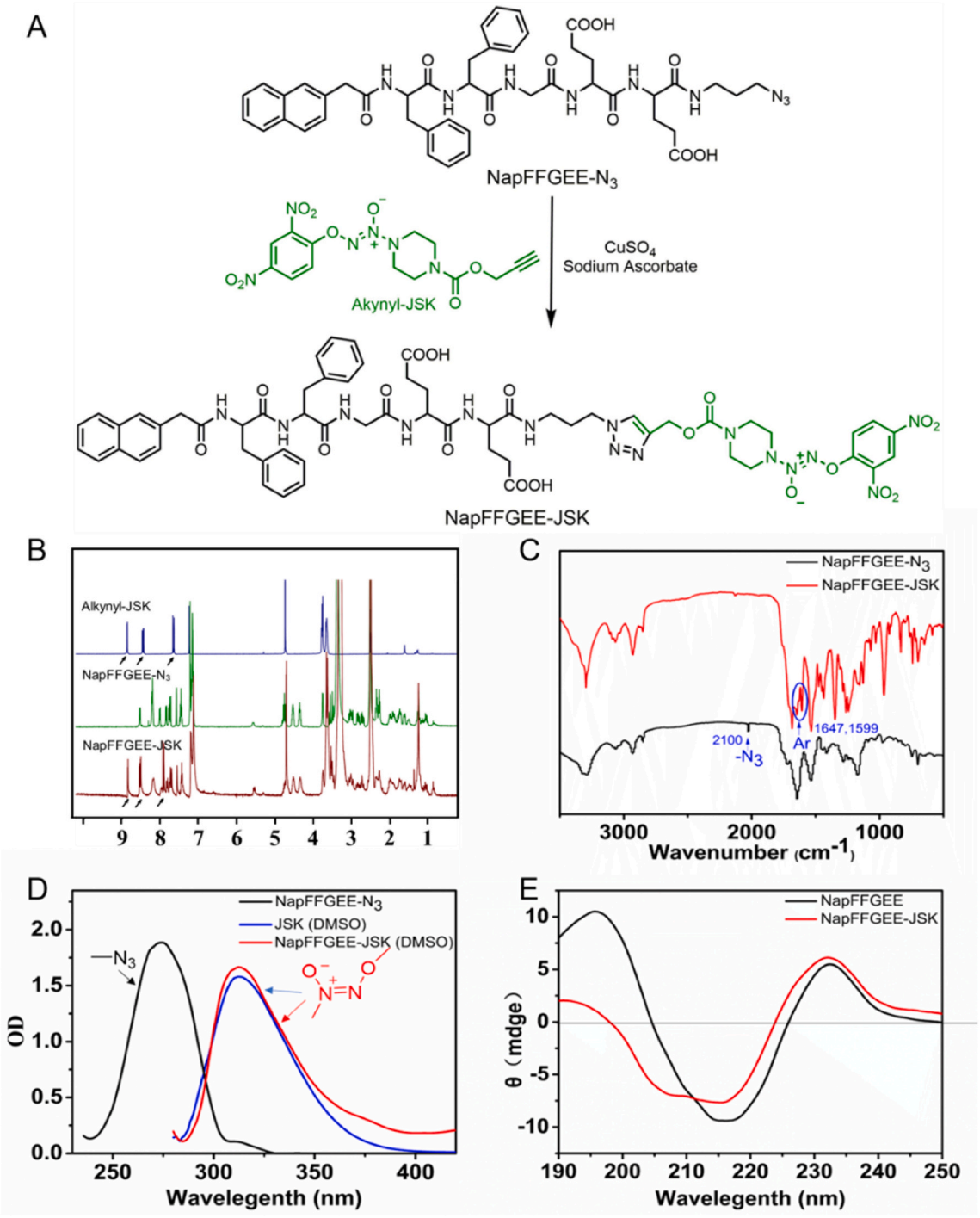

Fig. 1. The synthesis and characterization of NapFFGEE-JSK peptide. (A) Synthetic route of NO-prodrug conjugated NapFFGEE-JSK peptide. (B) ^{1}H NMR, (C) ATR-FTIR, (D) UV spectra and (E) CD spectra of NapFFGEE-N_3 and NapFFGEE-JSK, respectively.

designed by introducing double glutamic acids (EE) into the N-terminal of the sequence, which was expected to serve as the nano-carrier for alkynyl-JSK by self-assembly into supramolecular hydrogel. As illustrated in Fig. 1A, NapFFGEE peptide was synthesized by SPPS method [43,44], which was followed by the condensation reaction-mediated coupling between 3-azido-1-propanamine and NapFFGEE, yielding N_3-NapFFGEE with good selectivity and conversion rate (~82%). Then, NO prodrug conjugated peptide NapFFGEE-JSK was obtained by the Cu (I) catalyzed click reaction between azide group on N_3-NapFFGEE and alkyne group on JSK. The final product of NapFFGEE-JSK peptide was characterized by ^{1}H NMR, FTIR, UV–vis spectroscopy and Circular dichroism (CD), respectively. As shown in Fig. 1B, the characteristic magnetic resonance peak of alkynyl-JSK at 7.0–9.0 ppm assigned to the ArH of alkynyl-JSK could be clearly identified, indicating the successful conjugation of alkynyl-JSK onto NapFFGEE peptide. FTIR spectroscopy also verified the successful conversion of azide groups (Fig. 1C), where the characteristic absorption peak of $-N_3$ on the NapFFGEE-N_3 at 2100 cm^{-1} almost disappeared after click reaction, while two new peaks assigned to the benzene groups of alkynyl-JSK at 1647 cm^{-1} and 1599 cm^{-1} were clearly observed. In the UV–visible spectroscopy, the disappearance of the peak at 280 nm assigned to azide groups of N_3-NapFFGEE and the new absorption peak of diazeniumdiolate bonds at 300 nm of NapFFGEE-JSK confirmed the successful conjugation of alkynyl-JSK onto N_3-NapFFGEE (Fig. 1D). To further demonstrate the secondary structure of the peptide in aqueous solution, circular dichroism (CD) spectrum was obtained at a peptide concentration of 1 mg/mL. The results showed that similar β-sheet secondary structures with positive peaks at 195 nm and negative ones at 219 nm before or after alkynyl-JSK conjugation to NapFFGEE were observed (Fig. 1E), demonstrating that the alkynyl-JSK conjugation had no influence on the secondary structures of NapFFGEE. It was noticed that the ellipticity of NapFFGEE-JSK diminished after alkynyl-JSK conjugation, which was possibly attributed to the decrease of its water solubility, leading to low absorbance and curve fluctuation.

3.2. Preparation of NapFFGEE-JSK supramolecular hydrogel

Subsequently, the gelation ability of NapFFGEE-JSK peptide was evaluated. NapFFGEE-JSK (1 wt%) had poor solubility in phosphate-buffered saline (PBS, pH = 7.4) at room temperature, but it turned into a transparent solution upon increasing to 80 °C under ultrasound. After cooling to 25 °C, the transparent peptide solution transformed to opaque hydrogel within 5 min, which might be due to the self-assembly of NapFFGEE-JSK. The micro-structure of NapFFGEE-JSK hydrogel showed that the hydrogel was constituted by the enlaced and long nanofibers in diameters of 20–40 nm, in contrast to the amorphous aggregates in solution status (Fig. 2A). The formation of supramolecular nanofiber hydrogel might be due to the noncovalent hydrophobic and hydrogen bond interactions between NapFFGEE-JSK peptide [45]. Furthermore, we investigated the critical aggregation concentration (CAC) of NapFFGEE-JSK by DLS. The results showed that the CAC value of NapFFGEE-JSK was significantly lower than that of NapFFGEE, which should be attributed to the fact that the introduction of alkynyl-JSK facilitated the self-assembly behavior of NapFFGEE-JSK (Fig. 2B). Furthermore, compared with the UV absorption at 310 nm of NapFFGEE-JSK solution in DMSO, the UV adsorption of NapFFGEE-JSK nanofibers in PBS occurred at 352 nm, exhibiting obvious red-shift (Fig. 2C), clearly confirming the π–π stacking of the aromatic rings ascribed to alkynyl-JSK in the internal core of self-assembled nanofibers [46]. Finally, we employed rheometer to characterize the mechanical properties of the hydrogel at 37 °C. The values of storage moduli (G′) were five times higher than loss moduli (G′′) (Fig. 2D), confirming the formation of stable and homogeneous hydrogel. The storage modulus of the hydrogel was about 400 Pa, due to the low strength of the hydrogel, it could be in favor of peritumoral tumor injection through suitable syringe. Collectively, these results confirmed the successful self-assembly of NapFFGEE-JSK peptide into supramolecular hydrogel, which could serve as an efficient NO delivery platform.

3.3. GSH/GST-triggered NO release in vitro

In order to mimic the intracellular GSH/GST stimuli-triggered NO release, we evaluated the NO release manner from the NapFFGEE-JSK hydrogel and alkynyl-JSK in PBS with the presence of GSH/GST (Fig. 3A). As displayed in Fig. 3B, the maximal absorbance at 326 nm attributed to alkynyl-JSK decreased sharply within 2 h after incubation with GSH (10 mM) and GST (5 μg/mL) at 37 °C, suggesting the quickly decomposition of small molecular NO prodrug. However, the absorbance at 326 nm of NapFFGEE-JSK hydrogel can still be detected even after incubation for 24 h. The decelerated the reaction between NapFFGEE-JSK hydrogel and GSH/GST may be attributed to the encapsulation of JSK into a hydrophobic core in the nanofibers, which restricted the interaction with GSH/GST. As shown in Fig. 3C, the NO release profiles of NapFFGEE-JSK gels demonstrated a time-dependent

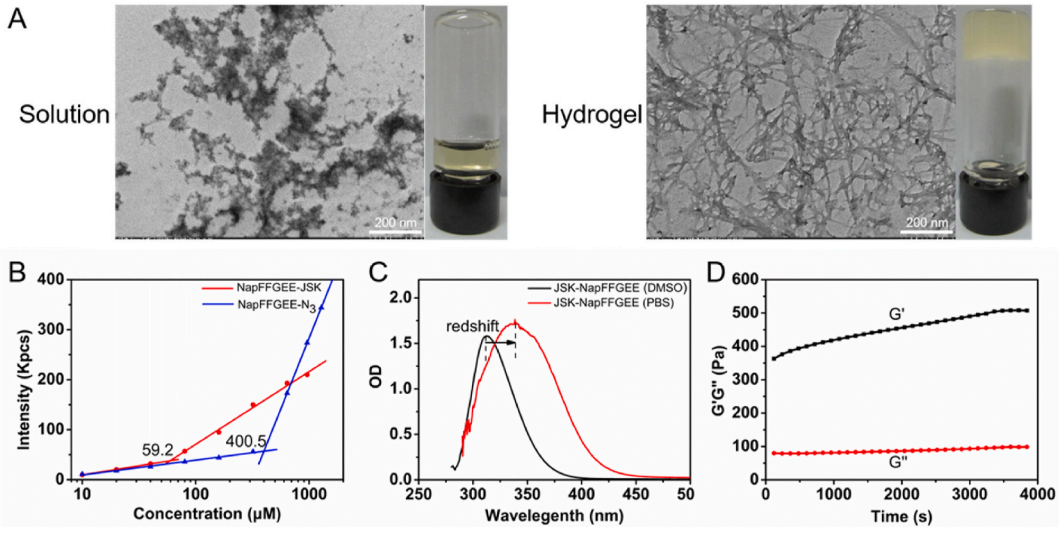

Fig. 2. The self-assembly of NapFFGEE-JSK peptide into supramolecular hydrogel. (A) TEM images of NapFFGEE-JSK (1 wt%) solution and corresponding supramolecular hydrogel after sol-gel transitions by heating-cooling process. (B) The CAC values of NapFFGEE-JSK and NapFFGEE-N_3 in PBS. (C) UV spectra of NapFFGEE-JSK peptide solution in DMSO and PBS. (D) The storage moduli (G′) and the loss moduli (G′′) of NapFFGEE-JSK hydrogel.

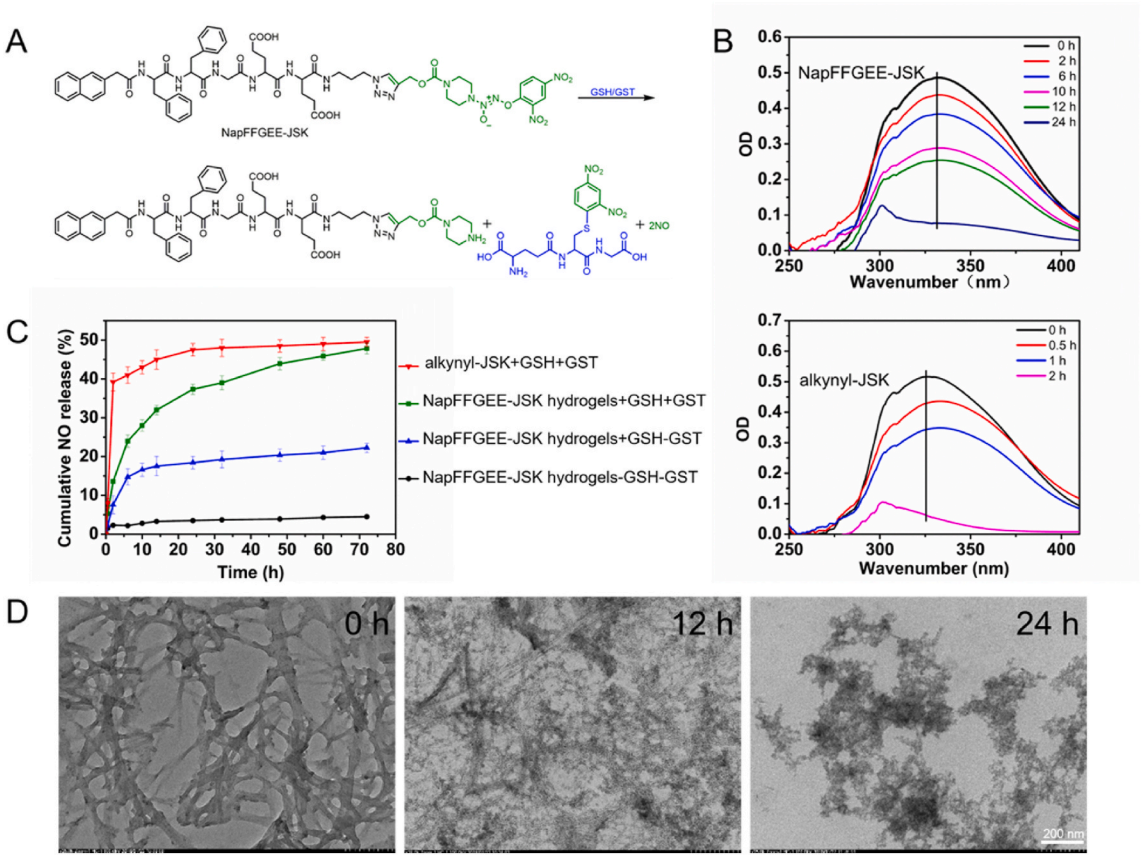

Fig. 3. GSH/GST-triggered NO release *in vitro*. (A) The chemical mechanism of GSH/GST responsive NO generation from NapFFGEE-JSK upon the nucleophilic attack by GSH and catalyzed by GST. (B) The time-dependent UV spectra after incubation NapFFGEE-JSK hydrogel or alkynyl-JSK (100 μM) with GSH (10 mM) and GST (5 μg/mL). (C) In vitro NO release of NapFFGEE-JSK hydrogel (100 μM) after treatment with various GSH and GST concentrations and determined with Griess reagent. (D) TEM images of NapFFGEE-JSK hydrogel (1 wt%) incubated in PBS containing GSH (10 mM) and GST (5 μg/mL) for 0, 12 and 24 h, respectively.

and sustained NO release profiles in the presence of GSH (10 mM) and GST (5 μg/mL), which could be extended to 72 h with cumulative NO release of approximately 47.85%. In contrast, the cumulative NO release in the other two control group of NapFFGEE-JSK gels without GSH/GST treatment or only with GSH (10 mM) treatment was 4.5% and 22.25%, respectively. These results indicated that the NO release from NapFFGEE-JSK should be triggered collaboratively by GSH and GST, which co-presented within cancer cells. In addition, we also assessed the cumulative NO release of NO prodrug, the results showed that alkynyl-JSK exhibited a rapid NO release behavior with 39.2% NO release in the first 6 h and 49.5% total NO release after 72 h, such rapid NO release fashion was difficult to maintain sustained cytotoxicity of NO against tumor cell. Notably, although the NO release rate of NapFFGEE-JSK hydrogels was delayed in comparation with alkynyl-JSK, the total cumulative NO release amount showed no significant difference. Therefore, this kind of NO release pattern of NapFFGEE-JSK hydrogel is expected to be beneficial for NO therapy with an effective dose in a prolonged time period. TEM images further revealed the influence of GSH/GST-responsive NO release on the morphology changes of NapFFGEE-JSK nanofibers (Fig. 3D), where swelling and rupture of the long nanofibers could be observed after treatment for 12 h, and even cracked into a lot of flocs after treatment for 24 h. The dis-assembly of NapFFGEE-JSK peptide with GSH/GST treatment may be attributed to the fact that the hydrophobic and hydrogen interaction was destroyed and the solubility of residual peptide was dramatically improved after NO release.

3.4. Intracellular NO release and in vitro cytotoxicity evaluation

To verify the self-assembled nanofibers of hydrogel can be internalized by cancer cell, the cellular uptake of FITC-labeled NapFFGEE (termed as NapFFGEE- FITC) was first evaluated by confocal laser scanning microscopy. After incubation MCF-7 ADR cells with NapFFGEE-FITC (5 μg mL^{-1}) for 4 h, obvious fluorescence from FITC-NapFFGEE (green) could be observed in the cytoplasm (Fig. S1), which suggested that the self-assembled nanofibers could be certainly internalized by MCF-7 ADR cancer cells through endocytosis [43]. The cancer drug candidate JSK, can be potentially activated by intracellular GSH/GST, which widely overexpressed inside tumor cells with about 1000 fold/10 fold higher than that of extracellular matrix, respectively [13,47]. Hence, for intracellular NO release, GSH/GST triggered NO release in the MCF-7 ADR cells was monitored by NO probe (4-amino-5-methylamino-2′,7′-difluorofluorescein diacetate, DAF-FMDA). As shown in Fig. 4A, obvious green fluorescent signal was obtained after treatment with NapFFGEE-JSK hydrogel for 4 h, suggesting that the successful intracellular release of NO. More intensive fluorescence was detected in the alkynyl-JSK group, which was mainly due to the rapid diffusion into cancer cell, which was also consistent with its rapid NO release *in vitro*. Meanwhile, no obvious fluorescence signal was observed for the cells treated only with the hydrogelator. The fluorescent intensity of NO was further quantificationally confirmed by flow cytometry, of which the signal intensity of cells treated with NapFFGEE-JSK was 1.21fold lower than alkynyl-JSK. It may be attributed to the slow endocytosis of supramolecular nanofibers. Subsequently, the intracellular sustained NO release of NapFFGEE-JSK hydrogel was tracked at 2 h, 6 h, 12 h, respectively. As illustrated in Fig. 4B, the fluorescence

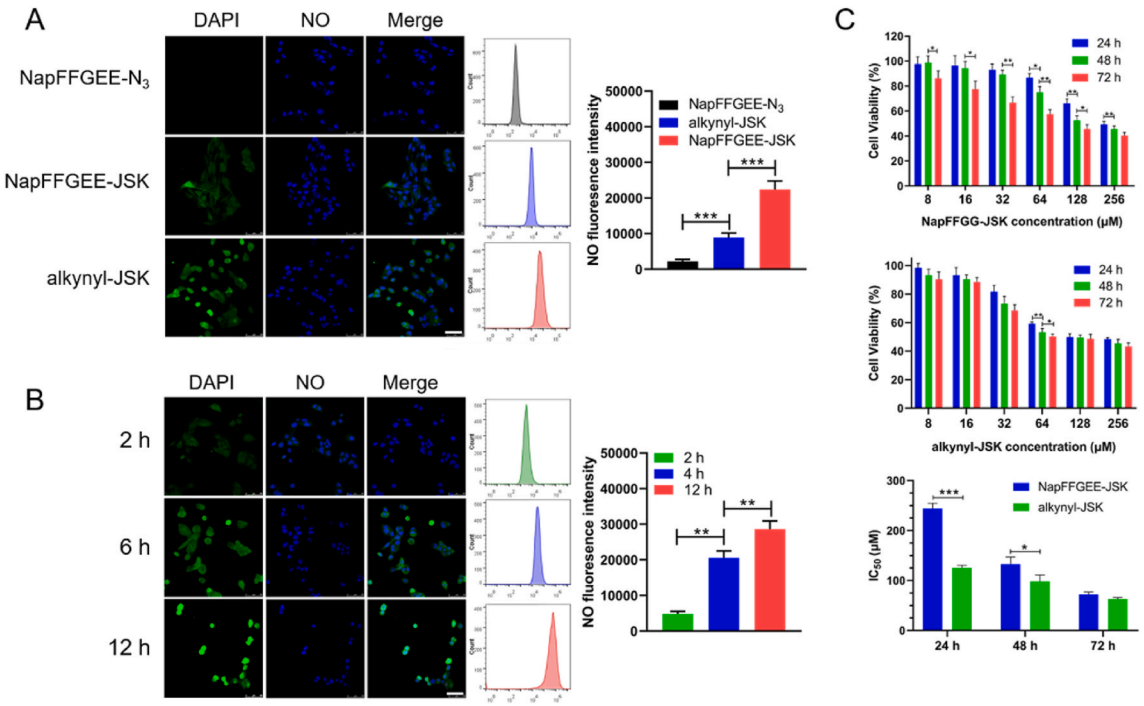

Fig. 4. Intracellular NO release and *in vitro* cytotoxicity evaluation. (A) Fluorescence microscopy images and Flow cytometer quantification of the MCF-7 ADR cells after incubation with NapFFGEE-N_3, alkynyl-JSK, NapFFGEE-JSK hydrogel for 4 h. (B) Fluorescence microscopy images and Flow cytometer quantification of the MCF-7 ADR cells after incubation with NapFFGEE-JSK hydrogel for 2 h, 6 h, and 12 h, respectively (NO, green; DAPI, blue). The scale bar is 25 μm. The data are expressed as Mean ± SDs (n = 3). (C) *In vitro* antitumor efficacy evaluation. The concentration was in range of 8–256 μM and the cytotoxicity was determined by CCK8 assay. And IC_{50} values of NapFFGEE-JSK hydrogel and alkynyl-JSK prodrugs for 24 h, 48 h, 72 h were calculated. $^*p < 0.05$, $^{**}p < 0.01$ and $^{***}p < 0.001$.

intensity gradually increased from 2 h to 12 h, indicating the sustained NO release in response to the overexpressed GSH/GST in the MCF-7 ADR cells. Flow cytometry analysis further quantificationally confirmed the sustained intracellular NO release profiles of NapFFGEE-JSK. Notably, an obvious morphological changes of cancer cell, membrane diffusion and nuclear shrinkage were observed at 12 h. It may be attributed to the fact that NO accumulation in cytoplasm and nuclei uniformly can induce cell apoptosis, which damage mitochondrial and DNA, respectively, resulting in the apoptosis and necrosis of MCF-7 ADR cells [18]. Hence, we further evaluated the antitumor activity of NapFFGEE-JSK against drug resistant MCF-7 ADR cell. According to Fig. 4C, the cell viability displayed concentration- and time-dependent patterns after treatment with both NapFFGEE-JSK hydrogel and JSK. The results showed that the IC_{50} for NapFFGEE-JSK hydrogel at 24, 48 and 72 h were 244.3, 132.66, 72.72 μM, respectively, while those for alkynyl-JSK were 125.3, 98.24 and 62.83 μM. The NO prodrug alkynyl-JSK showed a rapid tumor cell killing ability within 24 h and there was almost no increasement in the following 48 h. Notably, although the NapFFGEE-JSK hydrogel showed hysteretic cell cytotoxicity within 24 h in comparison with alkynyl-JSK, considerable treatment effect was obtained after incubation for 72 h, owing to the sustained NO release from supramolecular NapFFGEE-JSK hydrogel.

Furthermore, to investigate the selective anti-proliferative activity of NapFFGEE-JSK hydrogel against MCF-7 ADR cells, the cytotoxicity of NapFFGEE-JSK hydrogel on normal NIH/3T3 cells were studied (Fig. S2). The result showed that the cell viability was higher than 90% when the dose of the NapFFGEE-JSK was up to 245.78 μM, while the cell viability of MCF-7 ADR cells was below 20%. It was reasonable that the overexpressed GSH/GST (~1000/5 fold compared with normal cell) in MCF-7 ADR cells can trigger the intracellular NO release from NapFFGEE-JSK hydrogel, while it was difficult to trigger NO release in normal cell with much lower GSH/GST level. Collectively, the above results indicated the superior and selective inhibition effect of supramolecular hydrogel on MCF-7 ADR cell instead of normal cells.

3.5. *In vitro* apoptosis evaluation and mechanism assay

Generally, apoptosis is a major factor accounting for killing cancer cell. As shown in Fig. 5A, a total apoptosis rate of NapFFGEE-JSK hydrogel treatment group was 39.34% (29.4% and 9.94% for early and late apoptosis, respectively), while the alkynyl-JSK treatment group showed an apoptosis rate of 69.8% (52.2% and 17.6% for early and late apoptosis, respectively), which was in line with the cell cytotoxicity results. Subsequently, the apoptosis mechanisms were further elucidated. It has been reported that cell apoptosis was often induced by breaking the intracellular redox homeostasis [48,49]. Encouraged by the superior GSH consumptive fashion during the NO release and the excellent ROS production ability of NapFFGEE-JSK, it was expected that the GSH depletion could result in the amplification of intracellular oxidative stress and in sequence mediating NO-induced apoptosis of MCF-7 ADR cells. To verify this hypothesis, the GSH/GSSG level in MCF-7 ADR cells was monitored after receiving the treatment of NapFFGEE-JSK hydrogel and alkynyl-JSK for 48 h. As shown in Fig. 5B, the GSH/GSSG ratio of cell treated with NapFFGEE-JSK and alkynyl-JSK showed significant decrease, meanwhile ROS level exhibited significant increase. The GSH/GST responsive NO release mediated synchronous GSH depletion and ROS generation could induced directly intracellular oxidative stress amplification, which might result in mitochondrial dysfunction and subsequent mitochondria-mediated apoptosis. Therefore, we further measured the mitochondrial membrane potential and intracellular levels of ATP. As shown in Fig. 5C, significant decrease of mitochondrial membrane potential and intracellular ATP levels were observed.

Furthermore, we explore the mechanism underlying NO induced apoptosis by mitochondrion-mediated pathway, including the regulation of both pro-apoptotic proteins Bax and anti-apoptotic proteins Bcl-2 in mitochondria, the release of cytochrome *c* (Cyt *c*) from mitochondria into the cytoplasm and the finally activation of the apoptosis protein Caspase 9 and Caspase 3. We studied the apoptotic process by incubating

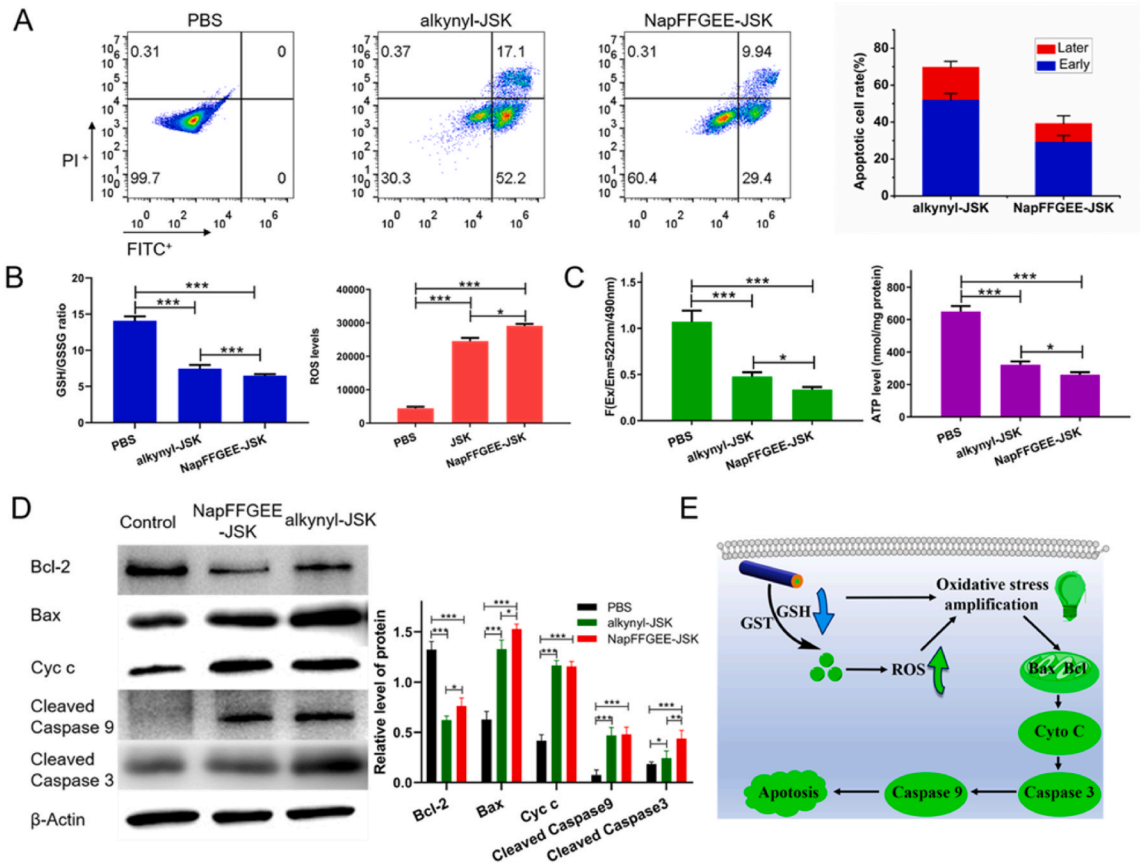

Fig. 5. ***In vitro*** **apoptosis evaluation and mechanisms assay.** (A) Annexin V-FITC/PI apoptotic staining for MCF-7 ADR cells treated with NapFFGEE-JSK hydrogel or alkynyl-JSK prodrug (62 μM) at 48 h was evaluated by flow cytometry analysis, the percentages of early or late apoptosis are presented in the bottom right and top right quadrants, respectively. And right columns represent the average proportions of apoptotic cells. (*$p < 0.05$, **$p < 0.01$, ***$p < 0.001$; n = 3). (B) Intracellular oxidative stress-elevation of NapFFGEE-JSK hydrogel or alkynyl-JSK treatment at 48 h *via* GSH/GSSG ratio and ROS levels assays. (C) Mitochondrial dysfunction induced by oxidative stress from NapFFGEE-JSK or alkynyl-JSK treatment for 48 h was accessed by the analysis of the mitochondrial membrane potential and ATP production. (D) Western blotting for the apoptosis proteins expression of Bcl-2, Bax, Cytochrome *c*, Cleaved Caspase 9 and Cleaved Caspase 3. The levels of protein expression were detected using specific antibodies and assayed by Image J software. The data are expressed as Mean ± SDs (n = 3). *$p < 0.05$; **$p < 0.01$, ***$p < 0.001$. (E) Schematic illustration of the mitochondrion mediated apoptotic mechanism of NapFFGEE-JSK supramolecular hydrogel on MCF-7 ADR cells.

MCF-7 ADR cells with NapFFGEE-JSK hydrogel or alkynyl-JSK for 48 h and then evaluated the related protein expression using western blot assay. The results revealed that NapFFGEE-JSK dramatically increased the relative expression level of pro-apoptotic Bax, Cyt C, Cleaved Caspase 3 and Cleaved Caspase 9 while reduced the expression level of anti-apoptotic Bcl-2 in MCF-7 ADR cells (Fig. 5D). Collectively, these results confirmed that NapFFGEE-JSK hydrogel induced MCF-7 ADR cell apoptosis by synergetic oxidative stress amplification-mediated mitochondrion apoptotic pathways (Fig. 5E).

3.6. Characterization of supramolecular hydrogel NapFFGEE-JSK/DOX and synergistic anticancer activity in vitro

Although the NO prodrug-based supramolecular hydrogel exhibited excellent antitumor efficiency on MCF-7 ADR cell, the cell viability was still up to nearly 40% at 72 h, indicating that the therapeutic effect needed to be further improved with combined agents. As reported, mounting evidences showed that NO could reverse drug resistance and enhance the sensitivity of chemotherapy by inhibiting P-gp expression and thus increasing drug accumulation in cancer cells NO [50,51]. DOX, a model chemotherapeutic drug for various kind of tumors, was employed in this study. As can be found in the peptide sequence, the EE amino acids with carboxylic acid (COOH) residues were used as the hydrophilic region of the NapFFGEE-JSK for tuning the hydrophile-lipophile balance, of which with the negative charges could interact electrostatically with DOX and contribute to the formation of supramolecular hydrogel (NapFFGEE-JSK/DOX) [52]. Hence, this supramolecular hydrogel was expected to provide a facile and effective platform for the codelivery of NO and DOX, which could achieve co-release by simultaneously response to the intracellular overexpressed GSH/GST and acid pH, respectively, aiming at obtaining synergistic therapeutic effect.

Firstly, the co-assembly behavior between DOX and NapFFGEE-JSK was investigated. Inverting vials experiment suggesting the loading of DOX with NapFFGEE-JSK and the successful preparation of supramolecular hydrogel (Fig. 6A). NapFFGEE-JSK/DOX hydrogel displayed the encapsulation efficiency of DOX was up to 85% and drug loading capacity was 4.2%. Given that DOX was interacted with the peptide by electrostatic interaction, we then investigated the zeta potential of NapFFGEE-JSK/DOX self-assembled nanofiber solution (0.1 wt%) diluted from NapFFGEE-JSK/DOX supramolecular hydrogel (1 wt %). The zeta potential of NapFFGEE-JSK/DOX nanofiber sharply decreased after the encapsulation of DOX (Fig. 6B), confirming the electrostatic interactions between amino group of DOX and carboxylic acid group of NapFFGEE-JSK. As showed in Fig. 6C, there was no significant changes of the storage modulus(G′) and loss modulus (G′′) after loading of DOX, indicating the DOX loading have negligible effect on the viscoelastic properties of the supramolecular hydrogel.

The release profiles of DOX from NapFFGEE/DOX hydrogel *in vitro* was then examined in PBS at different pH 7.4, 6.4 and 5.0 with GSH (10

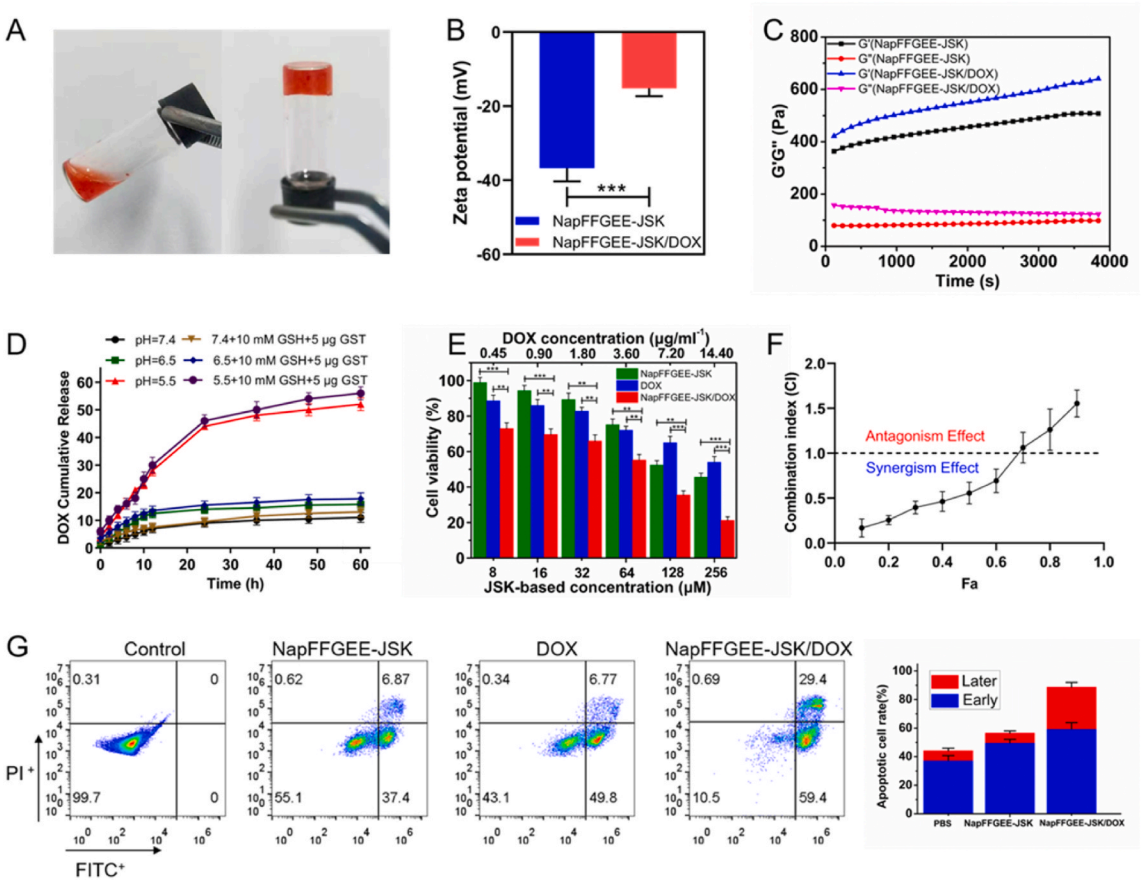

Fig. 6. Characterization of supramolecular hydrogel NapFFGEE-JSK/DOX and synergistic anticancer activity *in vitro*. (A) Optical images of NapFFGEE-JSK/DOX supramolecular hydrogel formed by mixing NapFFGEE-JSK (1 wt%) solution with DOX. (B) Zeta potentials of NapFFGEE-JSK/DOX nanofiber solution (0.1 wt%) diluted from NapFFGEE-JSK/DOX supramolecular hydrogel (1 wt%). (C) Rheological measurement in dynamic time sweep mode of JSK-NapFGEE/DOX (1 wt%) hydrogel and JSK-NapFGEE hydrogel. (D) In vitro pH sensitive DOX release from NapFFGEE-JSK/DOX hydrogel in PBS at different pH with GSH/GST. (E) *In vitro* cytotoxicity of NapFFGEE-JSK, DOX and NapFFGEE-JSK/DOX at 48 h. The JSK concentration was in range of 8–256 μM and DOX dose was various from 0.45 to 14.40 μg/mL. (F) Combination index (CI) values. (G) Cell apoptosis of MCF-7 ADR cells after treatment with PBS, NapFFGEE-JSK, DOX, NapFFGEE-JSK/DOX (62 μM).

mM) and GST (5 μg/mL), simulating the physiological environments of normal tissue and intracellular compartments, respectively. As shown in Fig. 6D, accelerated DOX release was observed upon decreasing pH values from 7.4 to 5.0. The amount of DOX release from the hydrogel in the presence of GSH (10 mM) and GST (5 μg/mL) was slightly higher than that of GSH/GST free group. It was shown that the release profile of DOX was pH-independent, which was slightly affected by NO release.

To evaluate the antitumor activity of NapFFGEE-JSK/DOX, the viability of the drug-resistant MCF-7 ADR cells treated with NapFFGEE-JSK, DOX, NapFFGEE-JSK/DOX for 48 h were assessed. As shown in Fig. 6E, although all three groups displayed concentration-dependent cytotoxicity on MCF-7 ADR cells, the NapFFGEE-JSK/DOX hydrogel group presented the much higher cytotoxicity than NapFFGEE-JSK hydrogel alone group or free DOX group, with the remaining cell viability at 48 h was 21.22%, 45.56%, 54%, respectively. The enhanced cytotoxicity of NapFFGEE-JSK/DOX should be attributed to the combined therapeutic effect of NO and DOX. According to combination index (CI) in Fig. 6F, when Fa<0.7, synergistic effects (CI < 1) was observed from the combination of NO and DOX therapy at 48 h, demonstrating the synergistic anticancer effect of NO and DOX against drug-resistant MCF-7 ADR cells. The apoptosis results obtained by flow cytometry was consistent with the *in vitro* anti-tumor activity, where the total apoptosis rate of NapFFGEE-JSK/DOX treatment was up to 94% (Fig. 6G), resulting in a significantly higher cell apoptosis rate compared with single treatment of NapFFGEE-JSK hydrogel or DOX.

3.7. Synergistic anticancer mechanism of NapFFGEE-JSK/DOX

The excellent antitumor effect of NapFFGEE-JSK/DOX encouraged us to consider the synergistic treatment mechanism against MDR cell. Fig. 7A depicts the feasible mechanism that NO might act as a chemosensitization agent by reverse P-gp-mediated drug resistance and increasing accumulation of intracellular DOX. Then, western blot analysis was used to access the expression of drug-resistant protein P-gp after treatment with NapFFGEE-JSK/DOX hydrogel for 24 h against MCF-7 ADR cells. As shown in Fig. 7B, compared to the control group and the free DOX group, the NapFFGEE-JSK/DOX hydrogel treated group with NO generation significantly down-regulated the expression of P-gp, which were 0.72 fold and 0.68 fold lower than that of DOX and negative control group. This result was also consistent with the results of ATP assay, since P-gp was a class of ATP energy-dependent transmembrane protein [16], which consumed the energy produced by hydrolysis of ATP to transfer the drugs out of cell. Subsequently, to further verify the inhibition effect of NO on efflux of drugs, the intracellular DOX level in MCF-7 ADR cells was monitored. As demonstrated in Fig. 7C, the DOX fluorescence signal was weak and mainly distributed in the cytoplasm instead of the nucleus. On the contrary, significantly stronger red fluorescence signals of DOX was found in the NapFFGEE-JSK/DOX hydrogel group, where DOX was mainly distributed in the nucleus, suggesting higher intracellular availability of DOX and excellent reversing effect of NO on MDR [53]. Flow cytometry analysis further confirmed the confocal data, where the fluorescence intensity of DOX in

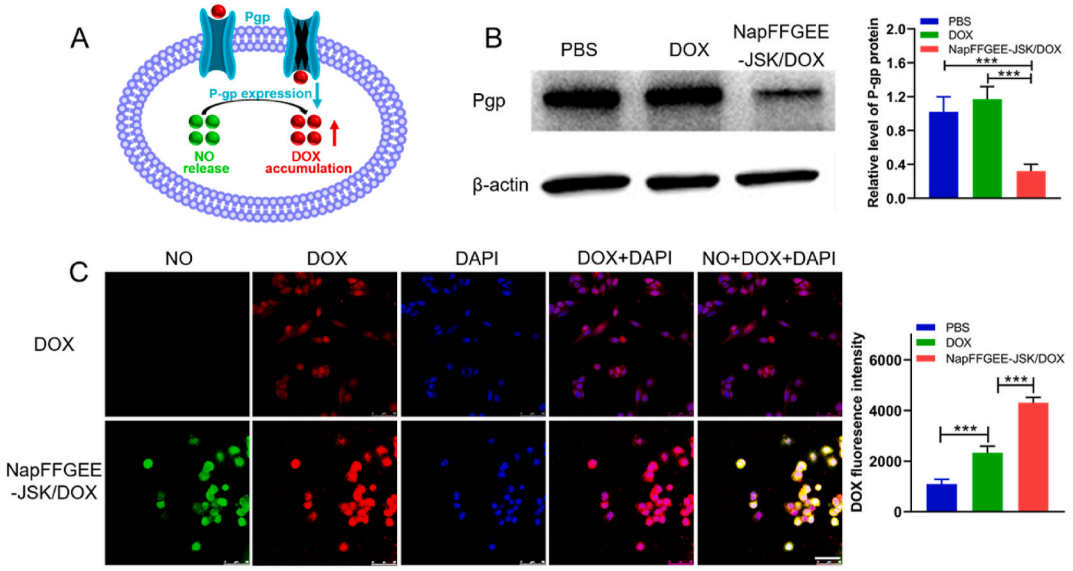

Fig. 7. Synergistic anticancer mechanism of NapFFGEE-JSK/DOX hydrogel. (A) Scheme illustration the chemosensitization effect of NO by downregulation P-gp expression and enhancing the intracellular accumulation of DOX. (B) Western blot and quantitative data of P-gp expression levels after treatment with PBS, DOX and NapFFGEE-JSK/DOX hydrogel (62 μM) for 24 h. (C) Confocal microscopy images and flow cytometric quantification after treatment with DOX and NapFFGEE-JSK/DOX hydrogel for 8 h (NO, green; DOX, red; DAPI, blue). The data were expressed as Mean ± SDs (n = 3), $*p < 0.05$, $**p < 0.01$ and $***p < 0.001$.

NapFFGEE-JSK/DOX group was 1.85 fold in comparison with that of free DOX. Overall, these results showed that the GSH/GST responsive NO release from NapFFGEE/DOX could effectively reverse the P-gp mediated MDR and improve DOX accumulation in MCF-7 ADR cells, which enhanced the chemosensitivity effect of DOX and achieved synergetic antitumor effect.

3.8. NO release and reverse DOX-resistant in vivo

In order to evaluate the NO release from the supramolecular hydrogel *in vivo*, immunofluorescence staining of tumor slices was conducted [54]. As shown in Fig. 8, peritumoral injection with NapFFGEE-JSK hydrogel or NapFFGEE-JSK/DOX hydrogel showed remarkably intensive fluorescence of NO compared with DOX and negative control group, indicating the efficient NO release within tumor *in vivo*. Next, to confirmed the NO released from the hydrogel could serve as efficient inhibitor for efflux pump P-gp, the expression of P-gp on the tumor cell was detected. Intense yellow fluorescence ascribed to P-gp was clearly observed in the cell membrane of DOX and control group, while the fluorescence signal and intensity of both NapFFGEE-JSK hydrogel and NapFFGEE-JSK/DOX hydrogel group were dramatically reduced, indicating that the NO release from the NapFFGEE-JSK hydrogel and NapFFGEE-JSK/DOX hydrogel treated group significantly down-regulated the expression level of P-gp. To

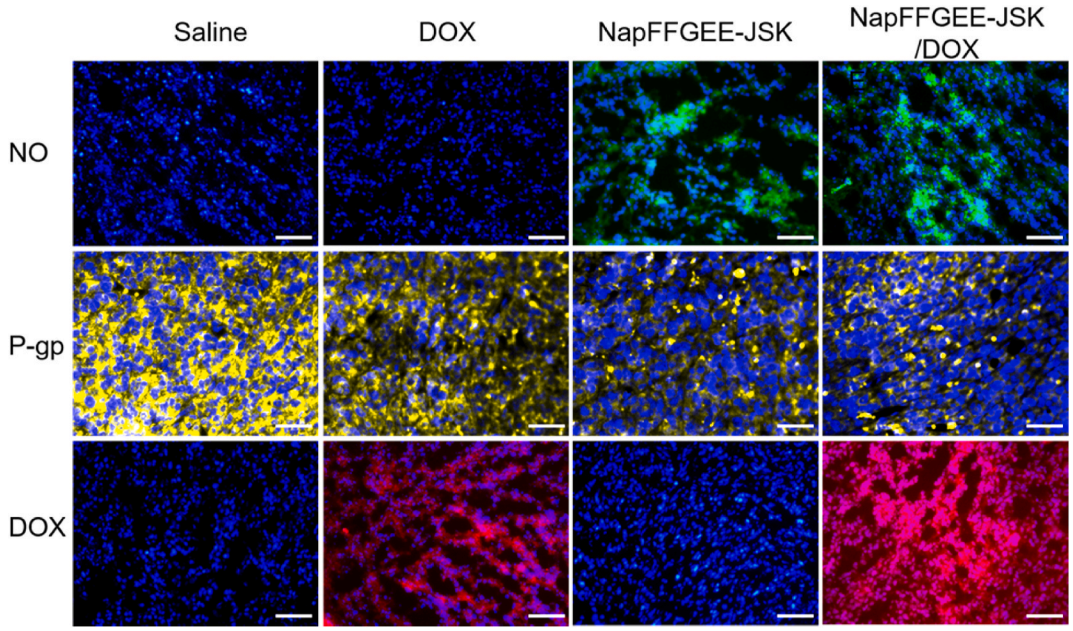

Fig. 8. NO release and reverse P-gp mediated DOX-resistant *in vivo*. Immunofluorescence images of tumor slices in the 2 mm^3 part of tumor tissue stained with anti-NT (standard indicator of NO *in vivo*), anti-P-gp antibody, respectively. And Alexa Fluor 488-labeled secondary antibody were added subsequently. NO, Pgp and DOX fluorescence signals were recorded by fluorescence microscope, respectively (NO, green; P-gp, yellow; DOX, red; DAPI, blue).

further confirm the effect of down-regulating P-gp expression on intracellular DOX accumulation, the tumor tissues slices were harvested. Slightly red fluorescence was observed in the mages of free DOX, which was mainly located in the cytoplasm instead of the cell nucleus, owing to the drug-resistant properties of MCF-7 ADR by pumping the majority DOX out of the tumor cell [55]. By contrast, in the NapFFGEE-JSK/DOX hydrogel treatment group, much stronger fluorescence signal especially in the cell nucleus was detected, which was expected to facilitate better therapeutic efficacy. Overall, the NapFFGEE-JSK/DOX hydrogel with NO releasing manner had a significant inhibition effect on the over-expression of P-gp, which was expected to reverse the MDR of tumor cells and enhance the chemosensitivity of DOX.

3.9. Antitumor activity in vivo

The *in vivo* antitumor efficacy of the NapFFGEE-JSK/DOX hydrogel was studied in NOD-SCID immune-deficient mice bearing MCF-7 ADR xenografts models. As displayed in Fig. 9A, NapFFGEE-JSK/DOX hydrogel treatment group demonstrated significant tumor suppression effect, suggesting the synergistic anticancer effect of NO and DOX based on NapFFGEE-JSK/DOX co-delivery systems. In addition, the tumor inhibition ratio was evaluated by isolating and weighting tumor tissues at the endpoint. The NapFFGEE-JSK/DOX hydrogel treatment group exhibited the significantly higher tumor inhibition rate (Fig. 9B). This excellent antitumor activity of NapFFGEE-JSK/DOX could be ascribed to two aspects: one was the locoregionally sustained release of NO and DOX in tumor situ, another was the reversion effect of NO on MDR of tumor. Besides, to evaluate the biosafety of NapFFGEE/DOX hydrogel *in vivo*, the body weight of the mice was monitored. No obvious body weight fluctuation was observed among the control, NapFFGEE-JSK and NapFFGEE-JSK/DOX group, indicating no severe side effects (Fig. 9C). By contrast, the free DOX group suffered from dramatic body weight loss up to 62%, during which one mouse died on the 10th day. The systemic toxicity of the tested formulations was further accessed by H&E staining of the main organs. As shown in Fig. S3, the organs of the NapFFGEE-JSK/DOX, NapFFGEE-JSK treated group showed no obvious sign of abnormity, indicating that the supramolecular hydrogel have good biosafety.

Furthermore, the histological changes of the tumor tissues after various treatments were evaluated though H&E staining (Fig. 9D). Compact cell arrangement was observed in control group receiving saline. On the contrary, the treatment with free DOX and NapFFGEE-JSK hydrogel induced partly necrosis of tumor cells with pyknotic and disappeared nuclei. In particular, the NapFFGEE-JSK/DOX group exhibited much more irregulated shaped necrotic regions in tumor sites, which presented the characteristics of cellular shrinkage and nuclear fragmentation. Immunohistochemical assays were conducted to access the expression of apoptosis-associated proteins, including Bcl-2, Bax and Caspase-3 in tumor tissues (Fig. 10). Cell positive to Bcl-2 and Bax markers illustrated blue-stained cell nuclei and brown blots in cytoplasm, while cells positive to caspase-3 displayed brown-stained nuclei and blue blots in cytoplasm. In NapFFGEE-JSK/DOX treatment group, the expression of pro-apoptotic protein Bax and anti-apoptotic protein Bcl-2 was considerably elevated and decreased, respectively, yielding signals of much more cell apoptosis [47]. The cleaved caspase-3 protein expressed the highest level in the NapFFGEE-JSK/DOX group, indicating the most activation of apoptosis. Subsequently, the TdT-mediated dUTP nick-end labeling (Tunel) staining also confirmed that NapFFGEE-JSK/DOX caused the most prominent apoptosis and cell death. Taken together, these results verified the synergistic treatment effect on MDR MCF-7 ADR tumor *in vivo* through the co-delivery of NO and DOX, based on a NO prodrug based supramolecular hydrogel delivery system.

Although ROS based treatments (including photodynamic therapy [56,57], sododynamic therapy [58,59], and chemodynamic therapy [60,61]) have been vastly developed for cancer therapy, NO has its own advantages by involving in various pathological processes [62]. In this study, JSK-based supramolecular hydrogel was facilely developed, which could significantly improve the bioavailability through locoregionally sustained NO release. Importantly, activated by the intracellular over-expressed GSH/GST, the JSK-based supramolecular hydrogel could induce the cascaded amplification of intracellular oxidative stress by the excellent production of reactive oxygen species (ROS) and superior consumption of GSH synchronously, resulting in significant antitumor efficiency by mitochondrion-mediated apoptotic pathways [49]. Meanwhile, it demonstrated chemosensitization effect by decreasing the P-gp expression levels, facilitating the intracellular and nuclear accumulation of DOX, resulting in significantly synergistic antitumor effect on drug-resistant breast cancer. Thus, our findings provided a new strategy to prepare NO prodrug nanomedicine and also a new type of intracellularly stimuli-sensitive NO delivery platform, which could be served as a local therapeutic depot for efficient chemotherapy, holding great potential for synergistically combating drug-resistance cancer.

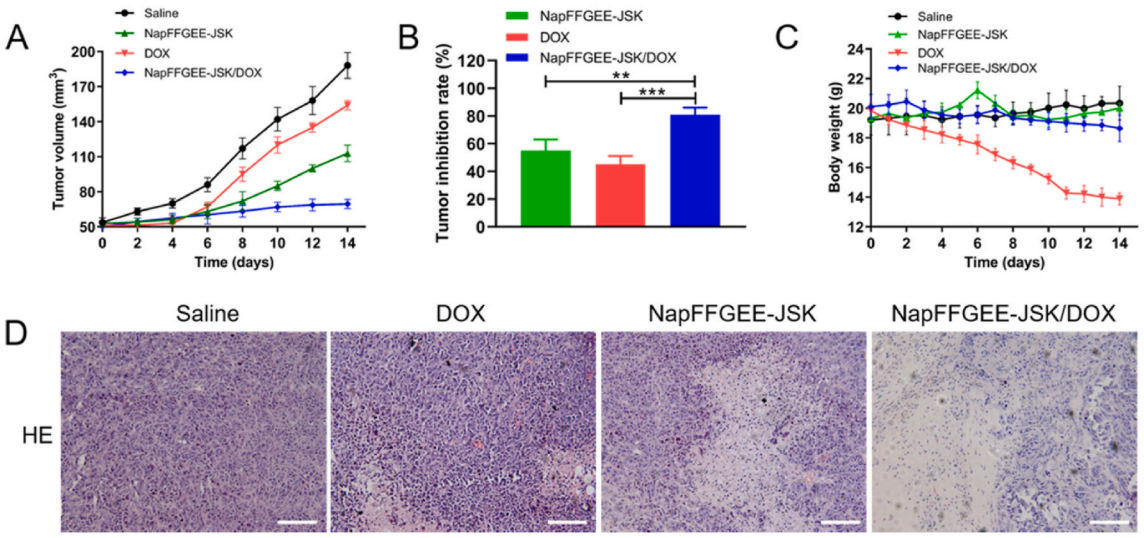

Fig. 9. *In vivo* antitumor efficacy evaluation and pathology assays. (A) Changes in relative tumor volume, (B) tumor inhibition rates and (C) body weight of mice with MCF-7 ADR tumors in response to different treatments. (D) The H&E (hematoxylin and eosin) analysis of MCF-7 ADR tumor tissue excised from the mice after receiving various treatments, nuclei are stained blue while extracellular matrix and cytoplasm are stained red. Scale bars: 50 μm.

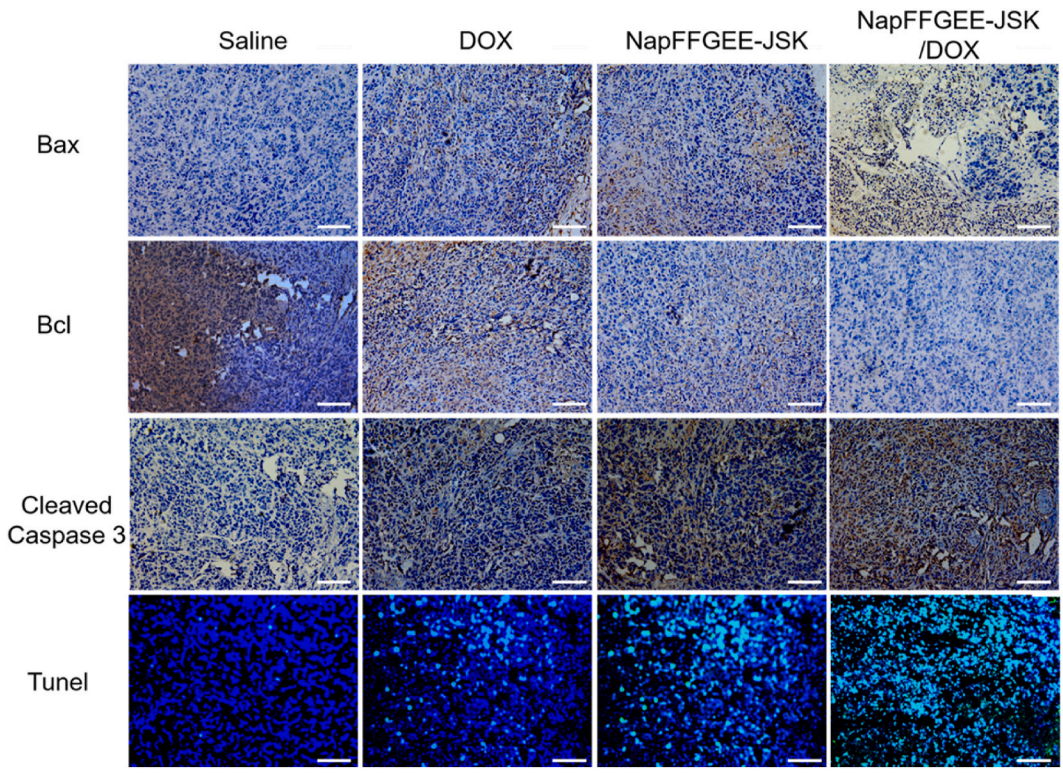

Fig. 10. Histology and immunohistochemistry assay of mitochondrion-mediated apoptotic protein *in vivo*. Tumor slices were stained with anti-Bax, anti-Bcl, anti-Cleaved Caspase 3 antibody for immunohistochemical-assay of mitochondrion mediated apoptotic protein. Tunel staining was conducted to evaluate apoptotic cells that undergo extensive DNA degradation. Cells were treated with saline, DOX, NapFFGEE-JSK and NapFFGEE-JSK/DOX, respectively. Scale bars: 50 μm.

4. Conclusion

In summary, we have successfully developed a kind of NO prodrug based-supramolecular hydrogel by self-assembly of NapFFGEE-JSK peptide. Due to the superior GSH depletion during GSH-consumption mediated NO release and the excellent ROS generation from NO, it synergetically amplified the intracellular oxidative stress and further induced mitochondrion mediated cell apoptotic pathway. Besides, this supramolecular hydrogel also provided a facile and effective codelivery platform for DOX, where the released NO could sensitize breast cancer cells to DOX by reversing the P-gp mediated MDR effect, achieving synergistic antitumor effect on drug-resistant breast cancer *in vivo*. Therefore, this GSH/GST-responsive NO prodrug based supramolecular hydrogel could be a promising platform for combating drug resistance in cancer chemotherapy.

CRediT authorship contribution statement

Jimin Zhang: Methodology, Validation, Investigation, Resources, Data curation, Writing – original draft, Visualization. **Meigui Deng:** Methodology, Validation, Formal analysis, Investigation, Resources, Visualization. **Xiaoguang Shi:** Software, Formal analysis. **Chuangnian Zhang:** Resources, Visualization. **Xiongwei Qu:** Data curation, Validation. **Xiuli Hu:** Funding acquisition, Supervision, Writing – review & editing. **Weiwei Wang:** Supervision, Funding acquisition, Writing – review & editing. **Deling Kong:** Project administration. **Pingsheng Huang:** Conceptualization, Writing – review & editing, Visualization, Funding acquisition.

Declaration of competing interest

The authors declare that they have no known competing financial interests or personal relationships that could have appeared to influence the work reported in this paper.

Acknowledgement

We acknowledge the financial support from the National Natural Science Foundation of China (No. U20A20260, 51973213), Natural Science Foundation of Hebei Province (C20202006). Tianjin Innovation Promotion Plan Key Innovation Team of Immunoreactive Biomaterials. Tianjin Innovation and Promotion Plan Key Innovation Team of Immunoreactive Biomaterials, and the Specific Program for High-Tech Leader & Team of Tianjin Government.

Appendix A. Supplementary data

Supplementary data to this article can be found online at https://doi.org/10.1016/j.bioactmat.2021.03.005.

References

[1] J.X. Yu, S. Upadhaya, R. Tatake, F. Barkalow, V.M. Hubbard-Lucey, Cancer cell therapies: the clinical trial landscape, Nat. Rev. Drug Discov. 19 (9) (2020) 583–584.
[2] J. Zhou, G. Yu, F. Huang, Supramolecular chemotherapy based on host-guest molecular recognition: a novel strategy in the battle against cancer with a bright future, Chem. Soc. Rev. 46 (22) (2017) 7021–7053.
[3] S. Agnello, M. Brand, M.F. Chellat, S. Gazzola, R. Riedl, A structural view on medicinal chemistry strategies against drug resistance, Angew. Chem. Int. Ed. 58 (11) (2019) 3300–3345.
[4] J. Tan, J. Tay, J. Hedrick, Y.Y. Yang, Synthetic macromolecules as therapeutics that overcome resistance in cancer and microbial infection, Biomaterials 252 (2020) e 120078.
[5] D.L. Chen, S.T. Ge, L.G. Zuo, S.H. Wang, M.L. Liu, S.Q. Li, Adjudin-loaded redox-sensitive paclitaxel-prodrug micelles for overcoming multidrug resistance with efficient targeted Colon cancer therapy, Drug Deliv. 27 (1) (2020) 1094–1105.
[6] M. Bar-Zeev, Y.D. Livney, Y.G. Assaraf, Targeted nanomedicine for cancer therapeutics: towards precision medicine overcoming drug resistance, Drug Resist. Updates 31 (2017) 15–30.

[7] J. Kim, B.C. Yung, W.J. Kim, X. Chen, Combination of nitric oxide and drug delivery systems: tools for overcoming drug resistance in chemotherapy, J. Contr. Release 263 (2017) 223–230.

[8] C.P. Liu, C.Y. Xie, J.X. Zhao, K.L. Ji, X.X. Lei, H. Sun, L.G. Lou, J.M. Yue, A. Dysoxylactam, A macrocyclolipopeptide reverses P-Glycoprotein-Mediated multidrug resistance in cancer cells, J. Am. Chem. Soc. 141 (17) (2019) 6812–6816.

[9] C.E. Soma, C. Dubernet, D. Bentolila, S. Benita, P. Couvreur, Reversion of multidrug resistance by co-encapsulation of doxorubicin and cyclosporin A in polyalkylcyanoacrylate nanoparticles, Biomaterials 21 (1) (2000) 1–7.

[10] H. Zhu, H. Chen, X. Zeng, Z. Wang, X. Zhang, Y. Wu, Y. Gao, J. Zhang, K. Liu, R. Liu, L. Cai, L. Mei, S.S. Feng, Co-delivery of chemotherapeutic drugs with vitamin E TPGS by porous PLGA nanoparticles for enhanced chemotherapy against multi-drug resistance, Biomaterials 35 (7) (2014) 2391–2400.

[11] X.R. Song, Z. Cai, Y. Zheng, G. He, F.Y. Cui, D.Q. Gong, S.X. Hou, S.J. Xiong, X. J. Lei, Y.Q. Wei, Reversion of multidrug resistance by co-encapsulation of vincristine and verapamil in PLGA nanoparticles, Eur. J. Pharmaceut. Sci. 37 (3–4) (2009) 300–305.

[12] M. Creixell, N.A. Peppas, Co-delivery of siRNA and therapeutic agents using nanocarriers to overcome cancer resistance, Nano Today 7 (4) (2012) 367–379.

[13] X.B. Jia, Y.H. Zhang, Y. Zou, Y. Wang, D.C. Niu, Q.J. He, Z.J. Huang, W.H. Zhu, H. Tian, J.L. Shi, Y.S. Li, Dual intratumoral redox/enzyme-responsive NO-releasing nanomedicine for the specific, high-efficacy, and low-toxic cancer therapy, Adv. Mater. 30 (30) (2018), e1704490.

[14] J.M. Zhang, H.J. Song, S.L. Ji, X.M. Wang, P.S. Huang, C.N. Zhang, W.W. Wang, D. L. Kong, NO prodrug-conjugated, self-assembled, pH-responsive and galactose receptor targeted nanoparticles for co-delivery of nitric oxide and doxorubicin, Nanoscale 10 (9) (2018) 4179–4188.

[15] K. Sharma, H. Chakrapani, Site-directed delivery of nitric oxide to cancers, Nitric Oxide 43 (2014) 8–16.

[16] Y.Y. Deng, F. Jia, X.H. Chen, Q. Jin, J. Ji, ATP suppression by pH-activated mitochondria-targeted delivery of nitric oxide nanoplatform for drug resistance reversal and metastasis inhibition, Small 16 (23) (2020), e2001747.

[17] S. Xu, G. Wang, Y. Lin, Y. Zhang, L. Pei, H. Yao, M. Hu, Y. Qiu, Z. Huang, Y. Zhang, J. Xu, Novel anticancer oridonin derivatives possessing a diazen-1-ium-1,2-diolate nitric oxide donor moiety: design, synthesis, biological evaluation and nitric oxide release studies, Bioorg. Med. Chem. Lett 26 (12) (2016) 2795–2800.

[18] W.P. Fan, B.C. Yung, X.Y. Chen, Stimuli-responsive NO release for on-demand gas-sensitized synergistic cancer therapy, Angew. Chem. Int. Ed. 57 (28) (2018) 8383–8394.

[19] Z. Huang, J. Fu, Y. Zhang, Nitric oxide donor-based cancer therapy: advances and prospects, J. Med. Chem. 60 (18) (2017) 7617–7635.

[20] Z.L. Huang, L. Liu, J.J. Chen, M.Y. Cao, J.G. Wang, JS-K as a nitric oxide donor induces apoptosis via the ROS/Ca2+/caspase-mediated mitochondrial pathway in HepG2 cells, Biomed. Pharmacother. 107 (2018) 1385–1392.

[21] M.J. Akhtar, M. Ahamed, H.A. Alhadlaq, S. Kumar, S.A. Alrokayan, Mitochondrial dysfunction, autophagy stimulation and non-apoptotic cell death caused by nitric oxide-inducing Pt-coated Au nanoparticle in human lung carcinoma cells, Biochimica et biophysica acta, General subjects 1864 (1) (2020), e129452.

[22] S.H. Li, X.R. Song, W. Zhu, Y.L. Chen, R. Zhu, L.P. Wang, X. Chen, J.B. Song, H. H. Yang, Light-switchable yolk-mesoporous shell UCNPs@MgSiO3 for nitric oxide-evoked multidrug resistance reversal in cancer therapy, ACS Appl. Mater. Interfaces 12 (27) (2020) e30066–30076.

[23] C.Y. Chu, X.M. Lyu, Z.X. Wang, H. Jin, S.Y. Lu, D. Xing, X.L. Hu, Cocktail polyprodrug nanoparticles concurrently release cisplatin and peroxynitrite-generating nitric oxide in cisplatin-resistant cancers, Chem. Eng. J. 402 (2020), e126125.

[24] M. Wan, H. Chen, Q. Wang, Q. Niu, P. Xu, Y. Yu, T. Zhu, C. Mao, J. Shen, Bio-inspired nitric-oxide-driven nanomotor, Nat. Commun. 10 (1) (2019) 966.

[25] R.R. Guo, Y. Tian, Y.J. Wang, W.L. Yang, Near-infrared laser-triggered nitric oxide nanogenerators for the reversal of multidrug resistance in cancer, Adv. Funct. Mater. 27 (13) (2017), e1606398.

[26] H. Yu, L.X. Cui, N. Huang, Z.L. Yang, Recent developments in nitric oxide-releasing biomaterials for biomedical applications, Med. Gas Res. 9 (4) (2019) 184–191.

[27] J. Hou, Y. Pan, D. Zhu, Y. Fan, G. Feng, Y. Wei, H. Wang, K. Qin, T. Zhao, Q. Yang, Y. Zhu, Y. Che, Y. Liu, J. Cheng, D. Kong, P.G. Wang, J. Shen, Q. Zhao, Targeted delivery of nitric oxide via a 'bump-and-hole'-based enzyme-prodrug pair, Nat. Chem. Biol. 15 (2) (2019) 151–160.

[28] P.X. Yang, H.J. Song, Y.B. Qin, P.S. Huang, C.N.A. Zhang, D.L. Kong, W.W. Wang, Engineering dendritic-cell-based vaccines and PD-1 blockade in self-assembled peptide nanofibrous hydrogel to amplify antitumor T-cell immunity, Nano Lett. 18 (7) (2018) 4377–4385.

[29] J. Gao, J. Zhan, Z. Yang, Enzyme-instructed self-assembly (EISA) and hydrogelation of peptides, Adv. Mater. 32 (3) (2020), e1805798.

[30] Z. Feng, X. Han, H. Wang, T. Tang, B. Xu, Enzyme-instructed peptide assemblies selectively inhibit bone tumors, Inside Chem. 5 (9) (2019) 2442–2449.

[31] Y.Z. Wang, C. Du, Y. Zhao, G.J. Nie, Y.M. Yang, Trap and kill strategy for non-BRCA mutant pancreatic cancer by co-delivery of olaparib and JQ1 with plectin-1 targeting peptide nanoparticles, Nano Today 33 (2020), e100877.

[32] H.J. He, S. Liu, D.F. Wu, B. Xu, Enzymatically formed peptide assemblies sequestrate proteins and relocate inhibitors to selectively kill cancer cells, Angew. Chem. Int. Ed. 59 (38) (2020) 16445–16450.

[33] K. Sato, M.P. Hendricks, L.C. Palmer, S.I. Stupp, Peptide supramolecular materials for therapeutics, Chem. Soc. Rev. 47 (20) (2018) 7539–7551.

[34] C.N. Fries, Y.Y. Wu, S.H. Kelly, M. Wolf, N.L. Votaw, S. Zauscher, J.H. Collier, Controlled lengthwise assembly of helical peptide nanofibers to modulate CD8(+)t-cell responses, Adv. Mater. 32 (39) (2020), e202003310.

[35] Z.J. Feng, Q. Su, C.N. Zhang, P.S. Huang, H.J. Song, A.J. Dong, D.L. Kong, W. W. Wang, Bioinspired nanofibrous glycopeptide hydrogel dressing for accelerating wound healing: a cytokine-free, M2-type macrophage polarization approach, Adv. Funct. Mater. 30 (52) (2020), e202006454.

[36] J. Gao, J. Zhan, Z.M. Yang, Enzyme-instructed self-assembly (EISA) and hydrogelation of peptides, Adv. Mater. 32 (3) (2020), e201805798.

[37] S.I. Stupp, On supramolecular self-assembly: interview with samuel stupp, Adv. Mater. 32 (20) (2020), e201906741.

[38] Z. Feng, H. Wang, B. Xu, Instructed assembly of peptides for intracellular enzyme sequestration, J. Am. Chem. Soc. 140 (48) (2018) 16433–16437.

[39] X.G. Shi, H.J. Song, C.R. Wang, C.N. Zhang, P.S. Huang, D.L. Kong, J.H. Zhang, W. W. Wang, Co-assembled and self-delivered epitope/CpG nanocomplex vaccine augments peptide immunogenicity for cancer immunotherapy, Chem. Eng. J. 399 (2020), e125854.

[40] Y. Zhang, Y. Kuang, Y.A. Gao, B. Xu, Versatile small-molecule motifs for self-assembly in water and the formation of biofunctional supramolecular hydrogels, Langmuir 27 (2) (2011) 529–537.

[41] Y.N. Shang, D.K. Zhi, G.W. Feng, Z.Y. Wang, D. Mao, S. Guo, R.H. Liu, L.L. Liu, S. H. Zhang, S.H. Sun, K. Wang, D.L. Kong, J. Gao, Z.M. Yang, Supramolecular nanofibers with superior bioactivity to insulin-like growth factor-I, Nano Lett. 19 (3) (2019) 1560–1569.

[42] B.C. Cheng, Y.F. Yan, J.J. Qi, L.F. Deng, Z.W. Shao, K.Q. Zhang, B. Li, Z.L. Sun, X. M. Li, Cooperative assembly of a peptide gelator and silk fibroin afford an injectable hydrogel for tissue engineering, ACS Appl. Mater. Interfaces 10 (15) (2018) 12474–12484.

[43] H.E. Xu, T.T. Wang, C.B. Yang, X.L. Li, G. Liu, Z.M. Yang, P.K. Singh, S. Krishnan, D. Ding, Supramolecular nanofibers of curcumin for highly amplified radiosensitization of colorectal cancers to ionizing radiation, Adv. Funct. Mater. 28 (14) (2018), e201707140.

[44] D.B. Zheng, Z.F. Gao, T.Y. Xu, C.H. Liang, Y. Shi, L. Wang, Z.M. Yang, Responsive peptide-based supramolecular hydrogels constructed by self-immolative chemistry, Nanoscale 10 (45) (2018) 21459–21465.

[45] J. Li, Y. Kuang, J.F. Shi, J. Zhou, J.E. Medina, R. Zhou, D. Yuan, C.H. Yang, H. M. Wang, Z.M. Yang, J.F. Liu, D.M. Dinulescu, B. Xu, Enzyme-instructed intracellular molecular self-assembly to boost activity of cisplatin against drug-resistant ovarian cancer cells, Angew. Chem. Int. Ed. 54 (45) (2015) 13307–13311.

[46] S. Sreejith, P. Carol, P. Chithra, A. Ajayaghosh, Squaraine dyes: a mine of molecular materials, J. Mater. Chem. 18 (3) (2008) 264–274.

[47] J. Fu, L. Liu, Z. Huang, Y. Lai, H. Ji, S. Peng, J. Tian, Y. Zhang, Hybrid molecule from O2-(2,4-dinitrophenyl)diazeniumdiolate and oleanolic acid: a glutathione S-transferase pi-activated nitric oxide prodrug with selective anti-human hepatocellular carcinoma activity and improved stability, J. Med. Chem. 56 (11) (2013) 4641–4655.

[48] R.W. Guo, G. Yang, Z.J. Feng, Y.J. Zhu, P.X. Yang, H.J. Song, W.W. Wang, P. S. Huang, J.H. Zhang, Glutathione-induced amino-activatable micellar photosensitization platform for synergistic redox modulation and photodynamic therapy, Biomaterials Science 6 (5) (2018) 1238–1249.

[49] Z.J. Feng, J.X. Guo, X. Liu, H.J. Song, C.N. Zhang, P.S. Huang, A.J. Dong, D. L. Kong, W.W. Wang, Cascade of reactive oxygen species generation by polyprodrug for combinational photodynamic therapy, Biomaterials 255 (2020), e120210.

[50] M.M. Chen, F.F. Song, Y. Liu, J. Tian, C. Liu, R.Y. Li, Q.Q. Zhang, A dual pH-sensitive liposomal system with charge-reversal and NO generation for overcoming multidrug resistance in cancer, Nanoscale 11 (9) (2019) 3814–3826.

[51] J. Fan, Q. He, Y. Liu, F. Zhang, X. Yang, Z. Wang, N. Lu, W. Fan, L. Lin, G. Niu, N. He, J. Song, X. Chen, Light-responsive biodegradable nanomedicine overcomes multidrug resistance via NO-enhanced chemosensitization, ACS Appl. Mater. Interfaces 8 (22) (2016) 13804–13811.

[52] F.H. Wang, H. Su, R. Lin, R.W. Chakroun, M.K. Monroe, Z.Y. Wang, M. Porter, H. G. Cui, Supramolecular tubustecan hydrogel as chemotherapeutic carrier to improve tumor penetration and local treatment efficacy, ACS Nano 14 (8) (2020) 10083–10094.

[53] Q. Song, S. Tan, X. Zhuang, Y. Guo, Y. Zhao, T. Wu, Q. Ye, L. Si, Z. Zhang, Nitric oxide releasing d-alpha-tocopheryl polyethylene glycol succinate for enhancing antitumor activity of doxorubicin, Mol. Pharm. 11 (11) (2014) 4118–4129.

[54] L.L. Tian, Y.X. Wang, L.L. Sun, J. Xu, Y. Chao, K. Yang, S. Wang, Z. Liu, Cerenkov luminescence-induced NO release from P-32-Labeled ZnFe(CN)(5)NO nanosheets to enhance radioisotope-immunotherapy, Matter 1 (4) (2019) 1061–1076.

[55] X. Zhang, G. Tian, W.Y. Yin, L.M. Wang, X.P. Zheng, L. Yan, J.X. Li, H.R. Su, C. Y. Chen, Z.J. Gu, Y.L. Zhao, Controllable generation of nitric oxide by near-infrared-sensitized upconversion nanoparticles for tumor therapy, Adv. Funct. Mater. 25 (20) (2015) 3049–3056.

[56] X.S. Li, S. Kolemen, J. Yoon, E.U. Akkaya, Activatable photosensitizers: agents for selective photodynamic therapy, Adv. Funct. Mater. 27 (5) (2017), e201604053.

[57] A. Kamkaew, S.H. Lim, H.B. Lee, L.V. Kiew, L.Y. Chung, K. Burgess, BODIPY dyes in photodynamic therapy, Chem. Soc. Rev. 42 (1) (2013) 77–88.

[58] J.J. Liu, M. Wu, Y.T. Pan, Y.K. Duan, Z.L. Dong, Y. Chao, Z. Liu, B. Liu, Biodegradable nanoscale coordination polymers for targeted tumor combination therapy with oxidative stress amplification, Adv. Funct. Mater. 30 (13) (2020) e 201908865.

[59] G. Canavese, A. Ancona, L. Racca, M. Canta, B. Dumontel, F. Barbaresco, T. Limongi, V. Cauda, Nanoparticle-assisted ultrasound: a special focus on sonodynamic therapy against cancer, Chem. Eng. J. 340 (2018) 155–172.

[60] Z.M. Tang, Y.Y. Liu, M.Y. He, W.B. Bu, Chemodynamic therapy: tumour microenvironment-mediated fenton and fenton-like reactions, Angew. Chem. Int. Ed. 58 (4) (2019) 946–956.
[61] Z.G. Ren, S.C. Sun, R.R. Sun, G.Y. Cui, L.J. Hong, B.C. Rao, A. Li, Z.J. Yu, Q.C. Kan, Z.W. Mao, A metal-polyphenol-coordinated nanomedicine for synergistic cascade cancer chemotherapy and chemodynamic therapy, Adv. Mater. 32 (6) (2020), e201906024.
[62] Y.Y. Deng, F. Jia, S.Y. Chen, Z.D. Shen, Q. Jin, G.S. Fu, J. Ji, Nitric oxide as an all-rounder for enhanced photodynamic therapy: hypoxia relief, glutathione depletion and reactive nitrogen species generation, Biomaterials 187 (2018) 55–65.